MATERIALS SCIENCE

Nanoparticle delivery of *CD40* siRNA suppresses alloimmune responses by inhibiting activation and differentiation of DCs and macrophages

Jialiang Wang[1,2], Kuirong Mao[1,3,2], Xiuxiu Cong[1,2], Huizhu Tan[1,2], Chenxi Wu[1], Zheng Hu[1,2], Yong-Guang Yang[1,3,2,4]*, Tianmeng Sun[1,3,2,4]*

CD40 is an important costimulatory molecule expressed on antigen-presenting cells (APCs) and plays a critical role for APC activation, offering a promising therapeutic target for preventing allograft rejection. Here, we developed a biodegradable nanoparticle small interfering RNA delivery system (si*CD40*/NPs) to effectively deliver *CD40* siRNA (si*CD40*) into hematopoietic stem cells (HSCs), myeloid progenitors, and mature dendritic cells (DCs) and macrophages. Injection of si*CD40*/NPs not only down-regulated *CD40* expression in DCs and macrophages but also inhibited the differentiation of HSCs and/or myeloid progenitors into functional DCs and macrophages. Furthermore, si*CD40*/NPs treatment significantly prolonged allograft survival in mouse models of skin allotransplantation. In addition to reiteration of the role of *CD40* in APC activation, our findings highlight a previously unappreciated role of *CD40* in DC and macrophage differentiation from their progenitors. Furthermore, our results support the effectiveness of si*CD40*/NPs in suppressing alloimmune responses, providing a potential means of facilitating tolerance induction and preventing allotransplant rejection.

INTRODUCTION

Immunological rejection remains a major obstacle to allogeneic organ transplantation (*1*–*3*), the best therapeutic option for patients with end-stage organ failure (*4*, *5*). Dendritic cells (DCs) and macrophages are the major antigen-presenting cells (APCs) driving immune responses against the transplanted organs (*6*–*11*). Costimulatory molecules are essential for APCs to prime and activate T cells (*12*, *13*). The *CD40-CD40*L costimulatory pathway has been found to play a critical role in the regulation of immune responses during allograft rejection (*14*, *15*). Although anti-*CD40*L antibodies were shown to induce immune tolerance in animal models (*16*–*18*), clinical trials revealed that it is impractical to use these antibodies in patients because of thromboembolic complications resulting from their interaction with *CD40*L on activated platelets (*19*); hence, anti-*CD40* antibodies are under development (*20*, *21*). Thus, new strategies have been explored for blocking the *CD40-CD40*L pathway. Because the ligation of *CD40* is essential for promoting the cell survival and the maturation and activation of DCs and macrophages (*22*, *23*), effectively blocking the *CD40* signal may induce satisfactory immune tolerance to allograft transplantation.

RNA interference is a powerful tool for suppressing targeted gene expression in mammalian cells (*24*, *25*). However, targeted delivery of RNA-based therapeutics for allograft transplantation remains a challenge (*26*–*28*). In this study, we sought to use nanoparticles (NPs), a previously tested effective small interfering RNA (siRNA) delivery carrier (*29*–*31*), for inhibiting allograft rejection. We developed a poly(lactic-*co*-glycolic acid) (PLGA)–based biodegradable NP delivery system with high siRNA loading efficiency. Using this system, we achieved effective in vivo delivery of *CD40* siRNAs into the mature DCs and macrophages, their progenitors, and hematopoietic stem cells (HSCs). Injection of *CD40* siRNA–loaded NPs not only down-regulated *CD40* expression on mature DCs and macrophages but also inhibited their differentiation and maturation, leading to significant prolongation of skin allograft survival in mice. This study provides previously unidentified insights into the immunomodulatory effects of *CD40* and offers an effective strategy to treat allotransplant rejection.

RESULTS

si*CD40*/NPs down-regulate *CD40* expression in DCs and macrophages in vitro

Biocompatible cationic lipid–assisted poly(ethylene glycol) (PEG)–PLGA–based NPs (CLANs) were prepared according to a previously reported double emulsion method (*32*) and used to deliver siRNAs. We confirmed that CLANs are effective in encapsulating *CD40* siRNA, with an efficiency of ~87%, through charge interaction between siRNA and 1,2-dioleoyl-3-trimethylammonium-propane (DOTAP) in the formulation. Cryo–transmission electron microscopy (cryo-TEM) analysis revealed that si*CD40*-encapsulated NPs (si*CD40*/NPs) remained a spherical morphology (Fig. 1A) and had a similar hydrodynamic diameter (Fig. 1B and fig. S1A) and ζ potential (fig. S1, B and C) to the blank NPs. Electrophoresis confirmed that NPs are highly efficient in encapsulating siRNA as only little free si*CD40* was detected in the prepared si*CD40*/NPs solution (Fig. 1C).

We first determined the efficacy of CLANs to enter DCs and macrophages using fluorescent dye–labeled siRNA (Fluorescein amidite {FAM}-siRNA or Cy5-siRNA)–encapsulated NPs. After 2 hours of incubation, the internalization of FAM-siRNA/NPs by DC and macrophage cell line cells was examined using flow

[1]Key Laboratory of Organ Regeneration and Transplantation of Ministry of Education, Institute of Immunology, The First Hospital, Jilin University, Changchun, Jilin, China. [2]National-local Joint Engineering Laboratory of Animal Models for Human Diseases, Changchun, Jilin, China. [3]International Center of Future Science, Jilin University, Changchun, Jilin, China. [4]State Key Laboratory of Supramolecular Structure and Materials, Jilin University, Changchun, Jilin, China.
*Corresponding author. Email: tsun41@jlu.edu.cn (T.S.); yongg@jlu.edu.cn (Y.-G.Y.).

Fig. 1. siCD40/NPs down-regulate CD40 expression in DCs and macrophages in vitro. (**A**) Cryo-TEM image of siCD40/NPs. Scale bar, 200 nm. (**B**) Particle size distribution of siCD40/NPs measured by dynamic light scattering. (**C**) Gel retardation assay of siCD40/NPs with an N/P ratio of 1:15. The unencapsulated siCD40 was analyzed by agarose gel electrophoresis. (**D**) The reconstruction of z stacks (10 slices) in a three-dimensional representation of DC1.2 cells and RAW264.7 cells after incubation with Cy5-siRNA/NPs, blank NPs, or PBS control at 37°C for 2 hours. The siRNA was labeled with Cy5 (red), cell nuclei were stained with DAPI (blue), and the cytoskeleton was stained with phalloidin-FITC (green). Scale bar, 10 μm. (**E** and **F**) Relative levels of CD40 mRNA in DC1.2 cells (E) and RAW264.7 cells (F) upon treatment with siCD40/NPs blank NPs, Lipo/siCD40 (75 nM siCD40), or PBS control at 37°C for 24 hours were assayed by qPCR. The data were the average of two independent experiments. (**G** and **H**) CD40 protein expression in DC1.2 cells analyzed by Western blotting (G) and flow cytometry (H). DC1.2 were treated with siCD40/NPs, blank NPs, or PBS control at 37°C for 48 hours (n = 3 per group). (**I** and **J**) CD40 proteins in RAW264.7 cells analyzed by Western blotting (I) and flow cytometry (J). RAW264.7 were treated with siCD40/NPs, blank NPs, or PBS control at 37°C for 48 hours (n = 3 per group). Data are presented as the means ± SEM. *P < 0.05, **P < 0.01, ***P < 0.001, ****P < 0.0001. MFI, mean fluorescence intensity.
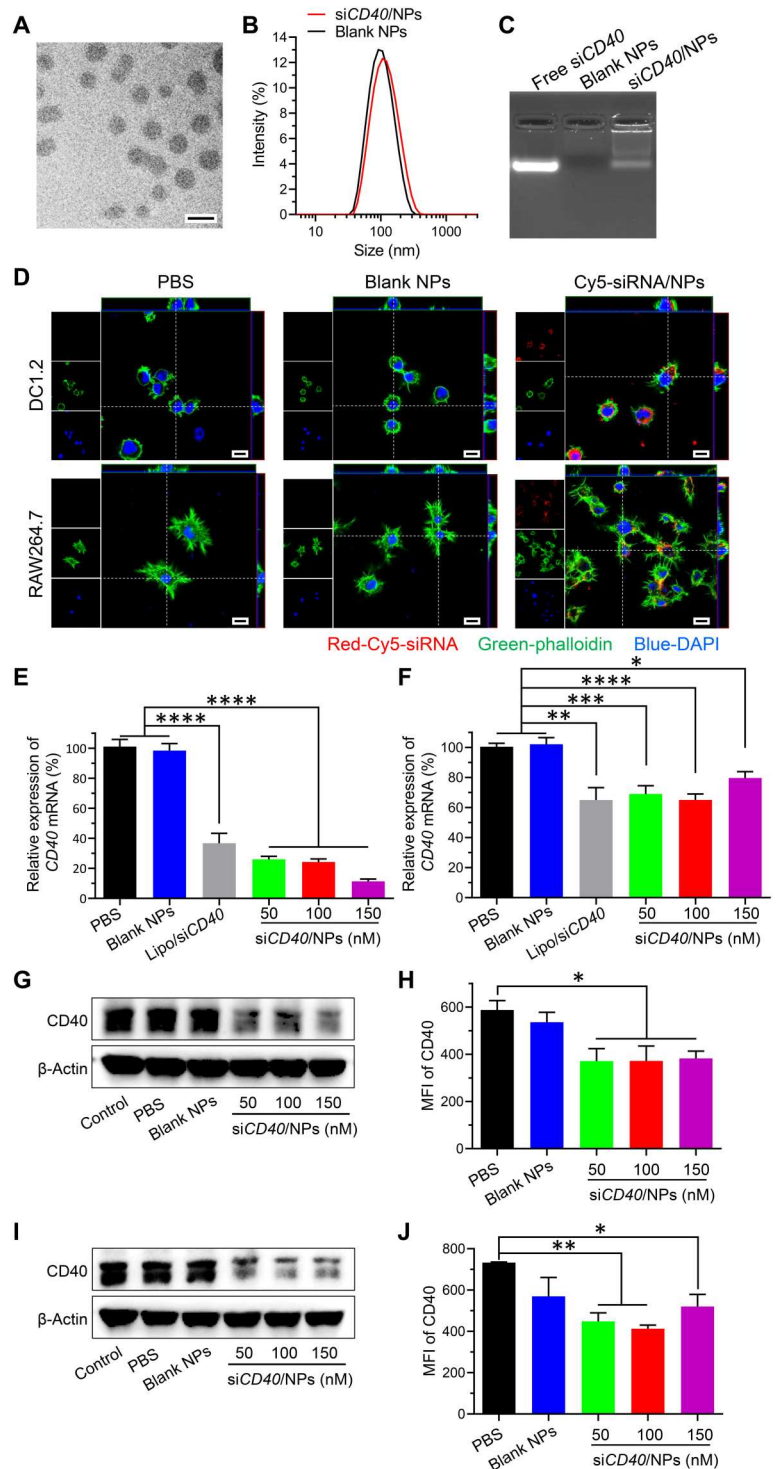
cytometry. Fluorescence signals were detected in DC (DC1.2) and macrophage (RAW264.7) cell line cells after incubation with FAM-siRNA/NPs (fig. S1, D to F) or with Cy5-siRNA (fig. S1, G to I), but not with blank NPs or free FAM-siRNA or Cy5-siRNA, compared to phosphate-buffered saline (PBS) control. The cells incubated with FAM-siRNA showed no significant reduction in fluorescence intensity after trypan blue treatment, which quenches extracellular

fluorescence (33), indicating that siRNA/NPs were endocytosed by DC1.2 and RAW264.7 cells (fig. S1, D to F). In line with these observations, intracellular fluorescence signals were firmly detected by confocal laser scanning microscopy (CLSM) in the cytoplasm of DC1.2 and RAW264.7 cells following incubation with Cy5-siRNA/NPs, but not with PBS or blank NPs (Fig. 1D and fig. S1J).

Then, we determined the efficacy of si*CD40*/NPs to inhibit *CD40* expression in vitro. Quantitative real-time polymerase chain reaction (qPCR) revealed that DC1.2 (Fig. 1E) and RAW264.7 (Fig. 1F) cells incubated with si*CD40*/NPs, but not those with blank NPs, showed a significant decrease in *CD40* mRNA levels compared to PBS control. The efficiency of si*CD40*/NPs to down-regulate *CD40* expression in DC1.2 cells (Fig. 1E) and RAW264.7 cells (Fig. 1F) was higher than and comparable to Lipo/si*CD40*, respectively. A significant decrease in *CD40* protein levels was also detected by Western blot and fluorescence-activated cell sorting (FACS) in si*CD40*/NP–, but not blank NP–treated DC1.2 (Fig. 1, G and H, and fig. S1K) and RAW264.7 (Fig. 1, I and J, and fig. S1L) cells compared to PBS control. These results indicate that si*CD40*/NPs can effectively down-regulate *CD40* expression in DCs and macrophages in vitro.

si*CD40*/NPs down-regulate *CD40* expression in splenic DCs and macrophages in vivo

We first examined si*CD40*/NPs delivery in DCs and macrophages in C57BL/6 mice 16 hours after intravenous injection of Cy5-si*CD40*/NPs or PBS (as control). IVIS imaging analysis revealed that strong Cy5 signals were found in the spleen and bone marrow (BM) cells from mice administered with Cy5-si*CD40*/NPs, but not in those of free Cy5-si*CD40*–injected mice, compared to PBS control (fig. S2, A and B). CLSM imaging demonstrated that in the spleen, Cy5 signals were predominantly localized in the red pulp and largely overlapped with CD11c^{+} or CD68^{+} cells (Fig. 2A). Flow cytometry analysis of CD11c^{+} DCs (Fig. 2B and fig. S2C) and F4/80^{+} macrophages (Fig. 2C and fig. S2C) in blood, spleen, and BM revealed that large proportions (50.74 to 78.76% for DCs and 50.06 to 73.18% for macrophages, respectively) of these cells were Cy5^{+}, confirming cellular uptake of Cy5-si*CD40*/NPs by DCs and macrophages in vivo, while very low levels of Cy5^{+} cells were detected in CD19^{+} B cells in blood, spleen, and BM from Cy5-si*CD40*/NP–treated mice (from 1.57 to 5.33%; fig. S2, D and E). These data indicate that si*CD40*/NPs are effective in delivering *CD40* siRNA to DCs and macrophages in mice after intravenous administration.

Next, we investigated the effects of si*CD40*/NPs on DCs and macrophages in C57BL/6 mice that were treated (intravenously) three times with si*CD40*/NPs every other day (control mice were injected with blank NPs or PBS with the same schedule; Fig. 3A). Mice injected with si*CD40*/NPs showed a significant decrease in the proportion and the amount of *CD40*^{+}CD11c^{high} cells (Fig. 3, B, C, and E) and *CD40*^{+}F4/80^{+} cells (Fig. 3, B, D, and F) in the spleens compared to PBS-injected controls. Furthermore, si*CD40*/NPs treatment also resulted in significant down-regulation of *CD40* expression on splenic CD11c^{+} (Fig. 3, G and H) and F4/80^{+} (Fig. 3, I and J) cells. No detectable difference in *CD40* expression was seen for CD11c^{+} or F4/80^{+} cells between blank NP– and PBS-injected mice. These data indicate that si*CD40*/NP treatment not only down-regulates *CD40* expression on DCs and macrophages but also results in a decrease in these cell populations in the spleen.

si*CD40*/NPs inhibit differentiation and maturation of DCs and macrophages

We next determined whether siRNA/NPs can be taken up by HSCs or progenitors and thereby affect the differentiation and maturation of DCs and macrophages. BM cells were harvested from C57BL/6 mice 16 hours after administration of Cy5-si*CD40*/NPs or PBS

and examined for Cy5-si*CD40* cellular uptake by Lin⁻Sca-1⁺c-Kit⁺ (LSK) cells, Lin⁻Sca-1^{low}c-Kit⁺FcγR^{low}CD34⁺ common myeloid progenitor (CMP), and Lin⁻Sca-1^{low}c-Kit⁺FcγR^{high}CD34⁺ granulocyte/macrophage progenitor (GMP) (fig. S3A). Flow cytometry (FCM) analysis revealed that Cy5⁺ cells were clearly detected in LSK cells (29.7 ± 2.1%), CMP (28.6 ± 3.8%), and GMP (60.0 ± 4.7%) from mice injected with Cy5-si*CD40*/NPs but almost undetectable in these cells from the PBS controls (Fig. 4, A and B). Cy5⁺ cells were also detected in CD11c⁺I-A/I-E⁻ DC progenitors (Fig. 4C and fig. S3B) and c-Kit⁺CD115⁺ monocyte progenitors (Fig. 4D and fig. S3B) in BM, blood, and spleen from Cy5-si*CD40*/NP–injected mice. These results indicate that siRNA/NPs provide an effective carrier for simultaneously delivering siRNA into DC and macrophage progenitor cells and precursor cells in vivo after intravenous injection.

Next, we investigated whether the si*CD40*/NPs can inhibit the differentiation of DCs and macrophages. C57BL/6 mice were administered with PBS, blank NPs, and si*CD40*/NPs by intravenous injection every other day for three times and 24 hours after the last injection, BM cells were harvested and examined for their potential to differentiate into mature DCs and macrophages (Fig. 5A). Briefly, BM-derived DCs (BMDCs) and macrophages (BMDMs) were differentiated from BM cells by culturing for 7 days with interleukin-4 (IL-4)/mouse granulocyte-macrophage colony-stimulating factor (mGM-CSF) or mM-CSF, respectively, followed by maturation with lipopolysaccharide (LPS) for 24 hours. FCM analysis revealed that BM cells from si*CD40*/NP–treated mice were less efficient than BM cells of PBS controls in differentiation into CD11c⁺ DCs (Fig. 5B and fig. S4A) and F4/80⁺CD11b⁺ macrophages (Fig. 5C and fig. S4B). Furthermore, DCs and macrophages differentiated from BM cells of si*CD40*/NP–treated mice also showed reduced activation by LPS, as shown by lower frequencies of activated CD86⁺I-A/I-E⁺ and CD40⁺ DCs (Fig. 5, D and E, and fig. S4A) as well as CD80⁺ and CD40⁺ macrophages (Fig. 5, F and G, and fig. S4B), compared to PBS control. Since there was no detectable difference in differentiation or activation of BMDCs or BMDMs between BM cells from blank NP– and PBS-injected mice, the observed effects of si*CD40*/NPs were considered to be a consequence of CD40 down-regulation.

In vitro assay was performed to directly assess the effect of si*CD40*/NPs on DC and macrophage differentiation. BM mononuclear cells were prepared and induced differentiation into DCs or macrophages in the presence of the same volume of PBS, blank NPs, si*NC*/NPs, or si*CD40*/NPs. We confirmed that, after being cultured with si*CD40*/NPs, the cellular uptake of si*CD40*/NPs by BM cells, including HSCs (LSK cells), CMPs, GMPs, monocyte progenitors, and DC progenitors, was highly efficient (fig. S5). The frequencies of mature and activated BMDCs and BMDMs after LPS stimulation were measured by flow cytometry (Fig. 6A). Compared to PBS control, frequencies of both total (CD11c⁺), activated (CD86⁺I-A/I-E⁺), and CD40⁺ BMDCs (Fig. 6, B to D, and fig. S6A) were significantly reduced in cultures added with si*CD40*/NPs but not with blank NPs or si*NC*/NPs. Similarly, the maturation and activation of LPS-stimulated BMDMs were markedly inhibited by si*CD40*/NPs, compared to PBS, blank NPs, and si*NC*/NPs (Fig. 6, E to G, and fig. S6B). In addition, treatment with si*CD40*/NPs resulted in a significant down-regulation of proinflammatory cytokines secreted in BMDCs (including *IL-1β*, *IL-6*, and *IL-12b*) and BMDMs [including tumor necrosis factor–α (*TNF-α*), *IL-1β*, *IL-6*,
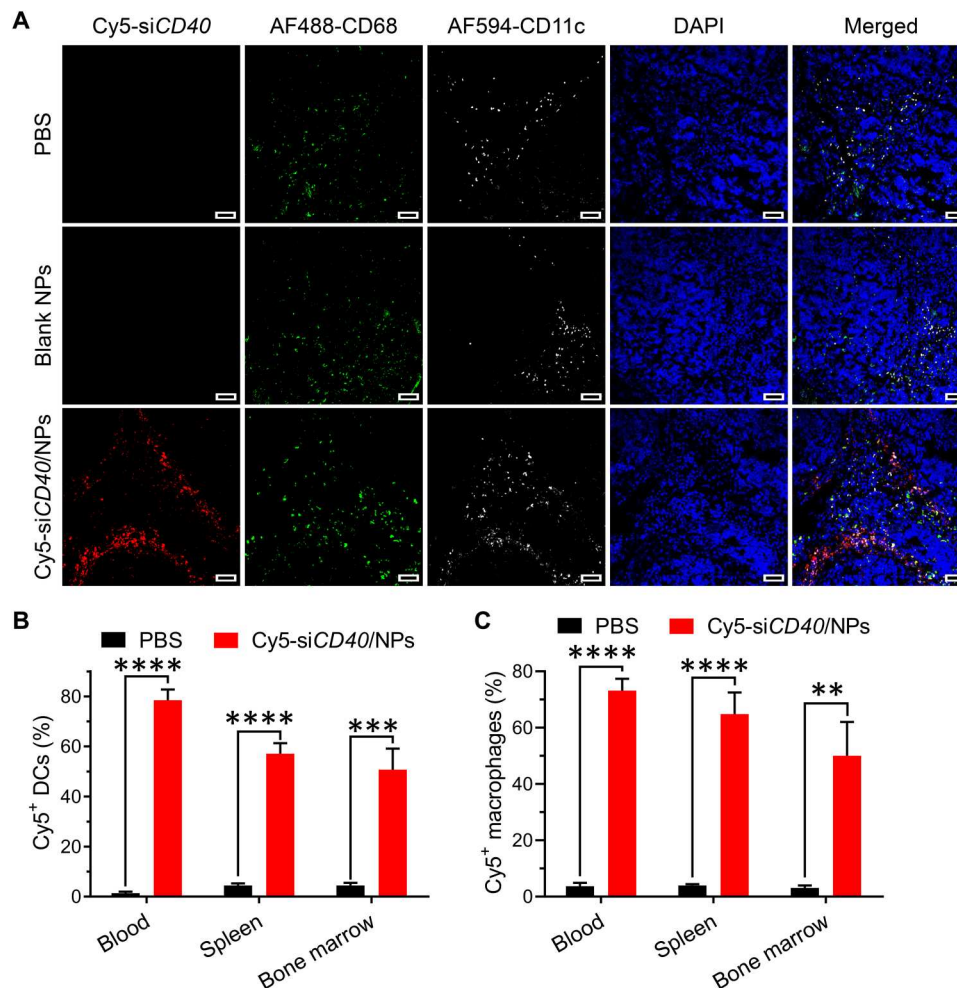
Fig. 2. si*CD40*/NPs simultaneously deliver *CD40* siRNA into DCs and macrophages in vivo. (**A**) CLSM images demonstrate the distribution of Cy5-si*CD40* in spleens of C57BL/6 mice administered (intravenously) with Cy5-si*CD40*/NPs, blank NPs, or PBS control. The siRNA was labeled with Cy5 (red), cell nuclei were stained with DAPI (blue), DCs were labeled with Alexa Fluor 594 anti-CD11c mAb (white), and macrophages were labeled with Alexa Fluor 488 anti-CD68 mAb (green). Scale bar, 50 μm. (**B** and **C**) Frequencies of Cy5⁺ DCs (B) and Cy5⁺ macrophages (C) measured by flow cytometry in leukocytes, splenocytes, and BM cells of C57BL/6 mice after intravenous injection of Cy5-si*CD40*/NPs or PBS control ($n = 6$ for PBS group, $n = 5$ for Cy5-si*CD40*/NPs group). Data are shown as the means ± SEM. **$P < 0.01$, ***$P < 0.001$, ****$P < 0.0001$.

and *IL-12b*] (fig. S7). These results indicate that si*CD40*/NPs can inhibit the differentiation of both DCs and macrophages from BM progenitor cells and maturation of the DCs and macrophages.

CD40 plays an important role in differentiation and maturation or activation of DCs and macrophages

Our results (Figs. 3, 5, and 6) suggest that *CD40* is likely requested for optimal differentiation and maturation or activation of DCs and macrophages. To confirm this possibility, we determined whether *CD40* down-regulation (by transduction with lentiviruses encoding *CD40* shRNA; fig. S8) in BM progenitors may also inhibit their potential to differentiate into DCs and macrophages. Briefly, BM cells were transduced with Lenti-sh*CD40* or non-coding short hairpin RNA (Lenti-sh*NC*) and then induced differentiation into BMDCs or BMDMs, as described above (Fig. 7A). FACS analysis confirmed that Lenti-sh*CD40* transduction was efficient in down-regulating *CD40* expression on *CD11c*⁺ BMDCs (Fig. 7, B to D). We found that BM cells transduced with Lenti-sh*CD40* were significantly

less efficient in differentiating mature DCs, as shown by reduced frequencies of total and mature (*CD86*⁺I-A/I-E⁺) *CD11c*⁺ DCs and levels of *CD11c* expression (Fig. 7, B and E to G) compared to Lenti-sh*NC*–transduced BM cells.

CD40 down-regulation had a similar effect on macrophage differentiation. Lenti-sh*CD40* transduction significantly down-regulated *CD40* expression on F4/80⁺*CD11b*⁺ BMDMs (Fig. 7, H to J). Lenti-sh*CD40*–transduced BM cells were significantly less efficient than those transduced with Lenti-sh*NC* in differentiation into F4/80⁺ macrophages (Fig. 7, H and K). Furthermore, BMDMs differentiated from Lenti-sh*CD40*–transduced BM cells showed poor activation in response to LPS stimulation, as shown by reduced *CD80* and F4/80 expression compared to those from Lenti-sh*NC*–transduced BM cells (Fig. 7, H, L, and M). Together, these results revealed an important role for *CD40* in differentiation and maturation or activation of DCs and macrophages, suggesting that si*CD40*/NPs may inhibit antigen presentation to T cells not
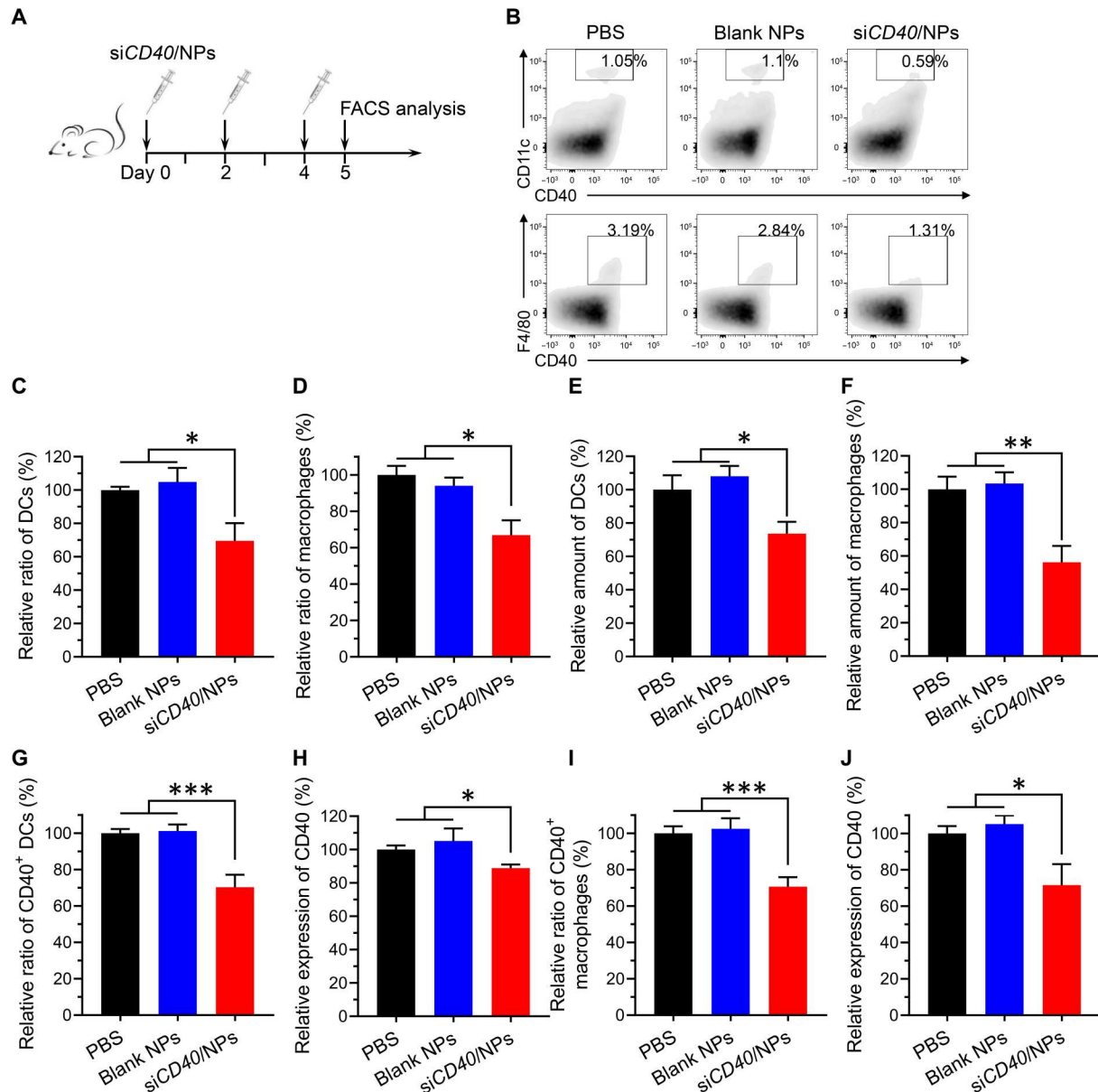
Fig. 3. si*CD40*/NPs hinder the differentiation and down-regulate *CD40* expression of DCs and macrophages in vivo. (**A**) Schematic of the overall design of C57BL/6 mice treated with si*CD40*/NPs, blank NPs, or PBS control. The dose of si*CD40* was 2.5 mg/kg body weight per injection. The splenocytes were analyzed by flow cytometry at 24 hours after the last injection. (**B**) Representative flow cytometry plots demonstrating frequencies of *CD40*+*CD11c*high DCs and *CD40*+F4/80+ macrophages in splenocytes. (**C** and **D**) Relative ratio of frequencies of *CD11c*high DCs (C) and F4/80+ macrophages (D) in splenocytes (*n* = 9 for the PBS group, *n* = 8 for the blank NPs group, and *n* = 7 for the si*CD40*/NPs group). (**E** and **F**) Relative amount of *CD11c*high DCs (E) and F4/80+ macrophages (F) in splenocytes (*n* = 9 for the PBS group, *n* = 8 for the blank NPs group, and *n* = 7 for the si*CD40*/NPs group). (**G** and **H**) Relative ratio of frequencies of *CD40*+ DCs (G) and in *CD40* levels in *CD11c*+ DCs (H) in splenocytes (*n* = 6 for the PBS group, *n* = 5 for the blank NPs group, and *n* = 4 for the si*CD40*/NPs group). (**I** and **J**) Relative ratio of frequencies of *CD40*+ macrophages (I) and *CD40* levels in F4/80+ macrophages (J) in splenocytes (*n* = 9 for the PBS group, *n* = 7 for the blank NPs group, and *n* = 8 for the si*CD40*/NPs group). Data are shown as the means ± SEM. *$P < 0.05$, **$P < 0.01$, ***$P < 0.001$.

only by directly targeting DCs and macrophages but also by inhibiting their differentiation and maturation from BM progenitors.

si*CD40*/NPs inhibit allograft rejection in mouse models of allogeneic skin transplantation

The efficacy of si*CD40*/NPs to inhibit alloimmune responses in vivo was first evaluated in a mouse model of major histocompatibility complex (MHC) class II mismatched skin allotransplantation. Briefly, C57BL/6 mice were treated with si*CD40*/NPs, blank NPs, or PBS (intravenous, every other day for nine times), and received skin transplantation from BM12 mice 5 days after the first injection of si*CD40*/NPs (Fig. 8A). Compared to PBS control, the survival of BM12 skin allografts was significantly prolonged in C57BL/6 mice treated with si*CD40*/NPs, but not with blank NPs (Fig. 8B and fig.
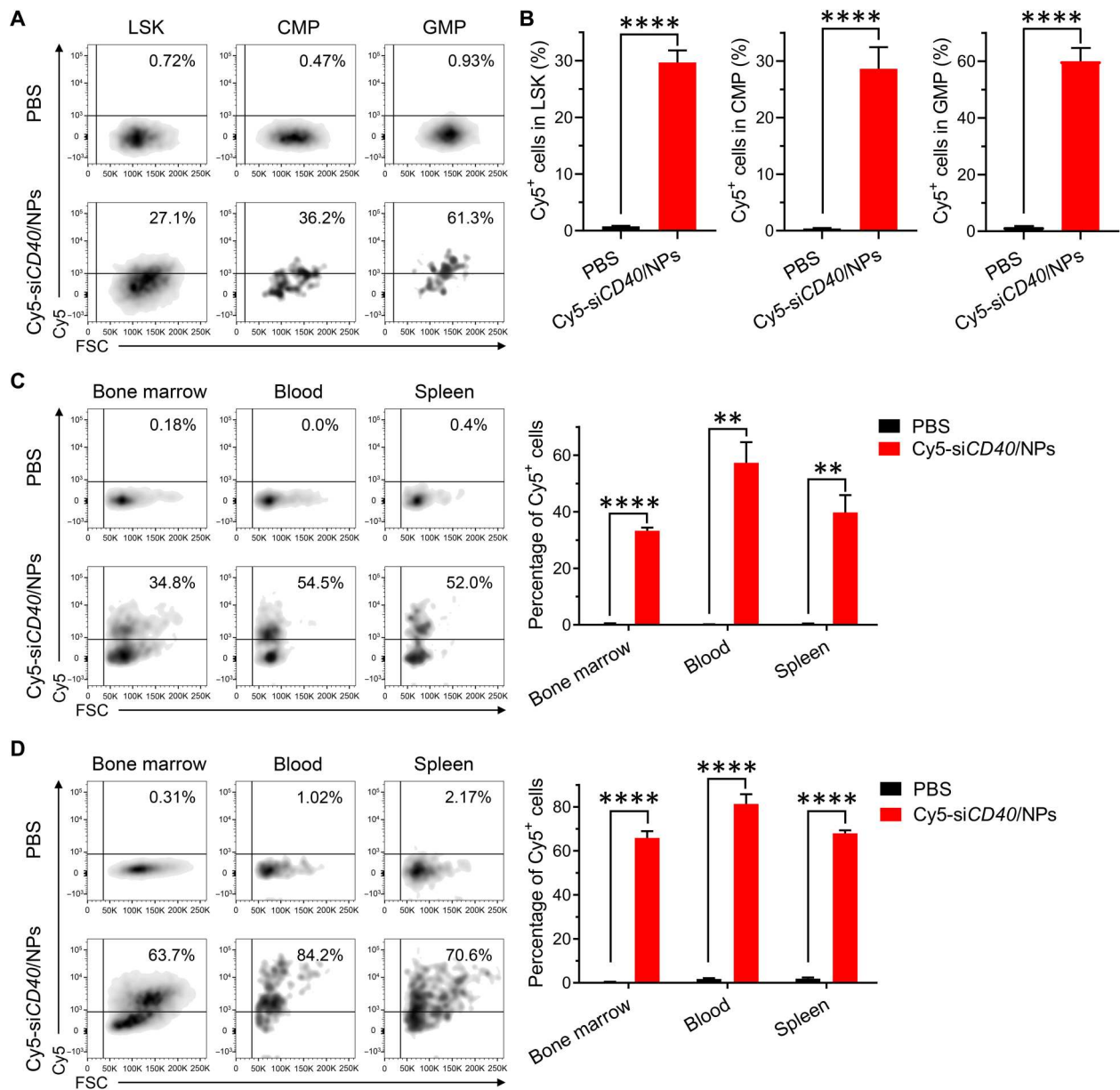
Fig. 4. siCD40/NPs simultaneously deliver CD40 siRNA into DCs, macrophages, and their progenitor cells in vivo. The mononuclear cells in blood, spleen, and BM of C57BL/6 mice were analyzed by flow cytometry at 16 hours after intravenous injection of Cy5-siCD40/NPs or PBS control. (**A**) Representative flow cytometry plots demonstrating Cy5+ cells in LSK cells, CMPs, and GMPs in BM cells of C57BL/6 mice after intravenous injection of Cy5-siCD40/NPs or PBS control. (**B**) Frequencies of Cy5+ cells in LSK cells (left), CMPs (middle), and GMPs (right) from BM of C57BL/6 mice after intravenous injection of Cy5-siCD40/NPs or PBS control ($n = 5$ per group). (**C**) Representative flow cytometry plots (left) and frequencies (right) of Cy5+ cells in DC progenitors in leukocytes, splenocytes, and BM cells from C57BL/6 mice after intravenous injection of Cy5-siCD40/NPs or PBS control ($n = 3$ per group). (**D**) Representative flow cytometry plots (left) and frequencies (right) of Cy5+ monocyte progenitors measured by flow cytometry in leukocytes, splenocytes, and BM cells from C57BL/6 mice after intravenous injection of Cy5-siCD40/NPs or PBS control ($n = 3$ per group). Data are presented as the means ± SEM. **$P < 0.01$, ****$P < 0.0001$.

S9A). We also measured anti-donor T cell responses by in vitro mixed lymphocyte reaction (MLR) assay, in which lymphocytes prepared from PBS-, blank NP-, or siCD40/NP–treated recipients 7 days after skin transplantation were used as the responders. Consistent with donor skin graft survival, lymphocytes from blank NP–treated recipients proliferated normally to the donor cells (fig. S9B) and the stimulator cells from BALB/c mice (third party; fig. S9C) compared to that of PBS control, while the lymphocytes from

recipients administered with siCD40/NPs showed significantly inhibited proliferative response not only to the donor stimulators (fig. S9B) but also to the third-party stimulators (fig. S9C). In line with skin allograft survival results, histological analysis revealed markedly reduced immune cell infiltration, vasculitis, thrombosis, and increase in thickness in skin allografts from siCD40/NP–treated mice compared to those from mice injected with PBS or blank NPs (fig. S9D).
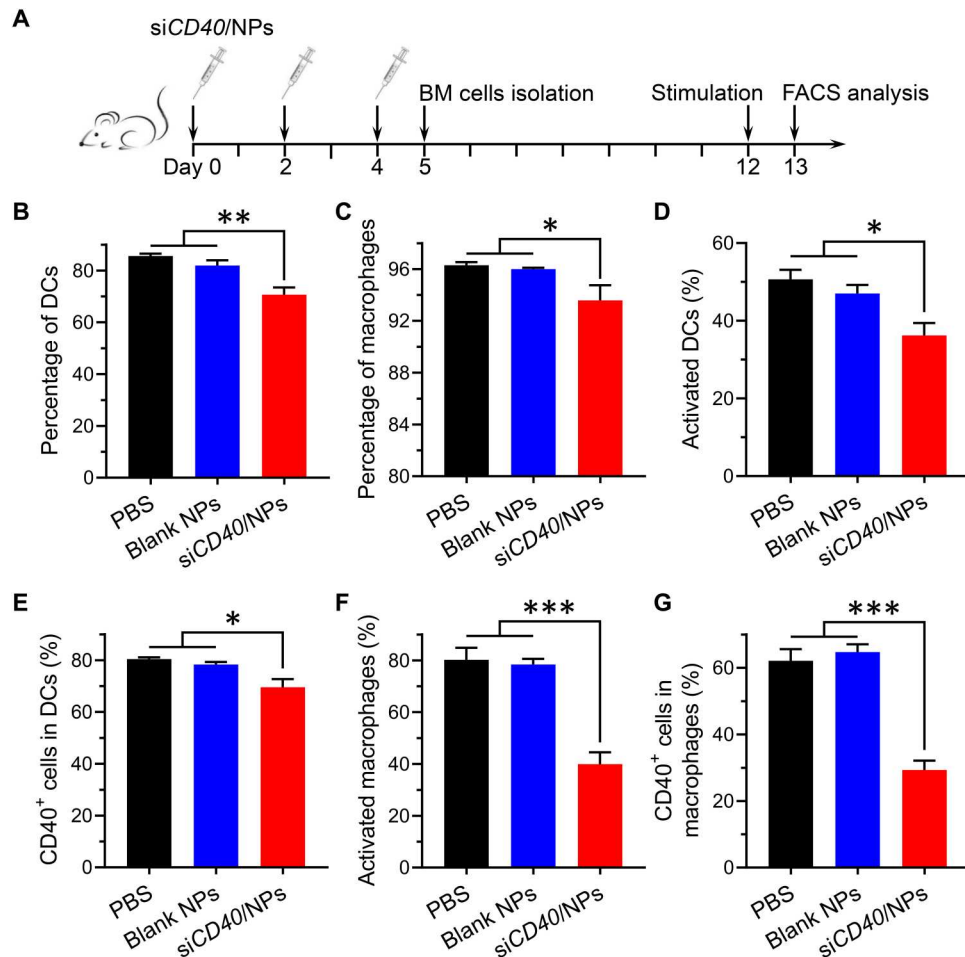
Fig. 5. si*CD40*/NPs hinder the differentiation and maturation of BMDCs and BMDMs ex vivo. (**A**) Schematic of the overall design of C57BL/6 treated with si*CD40*/NPs, si*NC*/NPs, blank NPs, or PBS control. C57BL/6 mice were administered with si*CD40*/NPs, blank NPs, or PBS control on days 0, 2, and 4 via intravenous injection. The dose of siRNA was 2.5 mg/kg body weight per injection. On day 5, the BM cells were isolated and cultured for induction of BM-derived DCs (BMDCs) and macrophages (BMDMs) using mIL-4 and mGM-CSF or mM-CSF, respectively. After culture for another 7 days, the BMDCs and BMDMs were stimulated with lipopolysaccharide (LPS) for 24 hours and analyzed by flow cytometry. (**B** and **C**) Frequencies of DCs (B) and macrophages (C) derived from BM cells of C57BL/6 mice ($n = 6$ per group). (**D** and **E**) Frequencies of matured DCs (D) and $CD40^+$ DCs (E) derived from BM cells of C57BL/6 mice ($n = 6$ per group). (**F** and **G**) Frequencies of matured macrophages (F) and $CD40^+$ macrophages (G) derived from BM cells of C57BL/6 mice ($n = 6$ for PBS and blank NPs groups and $n = 4$ for si*CD40*/NPs group). Data are presented as the means ± SEM. *$P < 0.05$, **$P < 0.01$, ***$P < 0.001$.

Encouraged by these results, we assessed whether si*CD40*/NPs, as a single agent, can inhibit skin allograft rejection in a fully MHC plus minor antigen−mismatched model, in which BALB/c mouse skin was grafted onto C57BL/6 mice 5 days after the first injection of si*CD40*/NPs, blank NPs, or PBS (Fig. 8A). As shown in Fig. 8C and fig. S9E, BALB/c skin allograft survival was significantly prolonged in si*CD40*/NP−treated C57BL/6 mice compared to those injected with PBS or blank NPs. In addition, we found that si*CD40*/NPs may act synergistically with rapamycin to further improve the survival time of BALB/c mouse skin allografts in C57BL/6 mice (Fig. 8D and fig. S9F).

To assess the toxicity of si*CD40*/NPs, histological analysis was performed on organs (brains, lungs, hearts, livers, spleens, and kidneys) from the recipient mice at the end of the experiments. Neither si*CD40*/NP− nor blank NP−treated mice showed detectable lesions in these organs (fig. S10A). We also found that si*CD40*/NP treatment did not significantly compromise antiviral immunity

when challenged with FM1 viruses 14 days after withdrawing the treatment (fig. S10, B to D). Together, these results indicate that si*CD40*/NPs provide a potentially safe and effective strategy to inhibit allograft rejection.

DISCUSSION
Blockade of *CD40-CD40L* signal pathway effectively inhibits the activation of alloreactive T cells, induces the expansion of regulatory T cells, and has been reported to be an effective approach to inducing immune tolerance in organ transplantation (*14*, *34*, *35*). In our study, we successfully silenced *CD40* expression in both DCs and macrophages in vivo using si*CD40*/NPs, a biocompatible NP siRNA delivery system with highly positive surface charge, resulting in significantly reduced activation of alloreactive T cells and improved survival of skin allografts in mice. We further found that unlike anti-*CD40* antibodies, si*CD40*/NPs could effectively inhibit
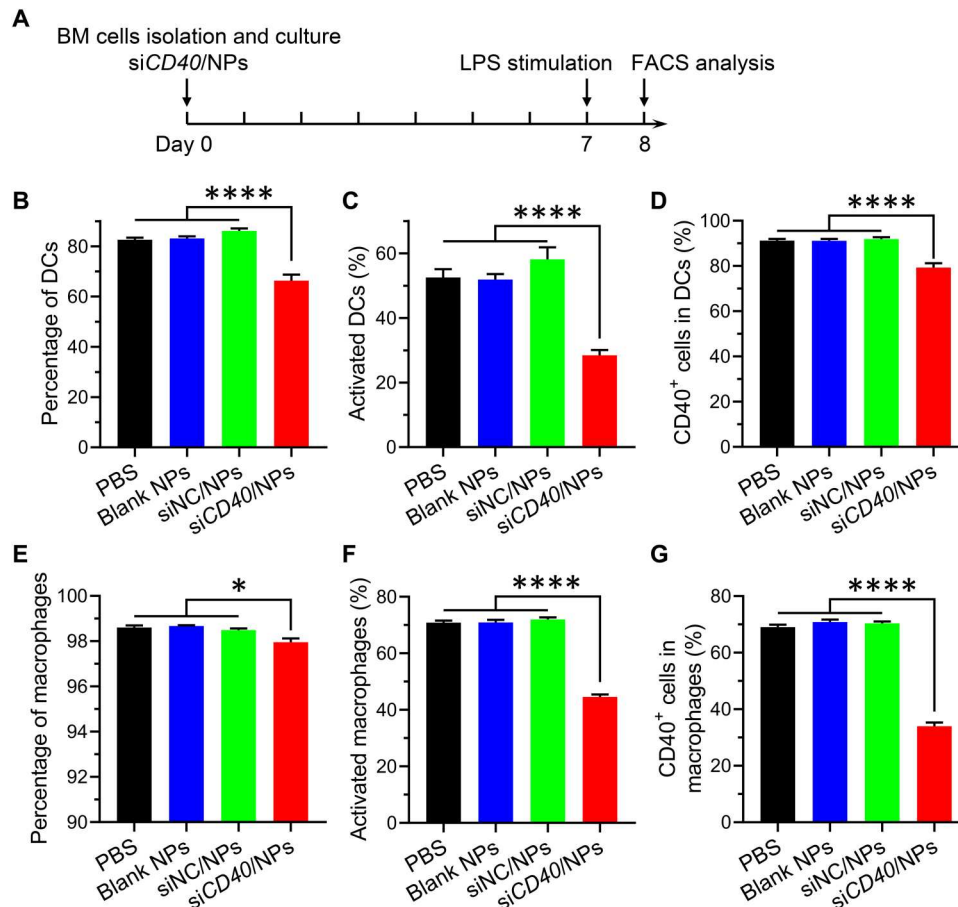
Fig. 6. si*CD40*/NPs hinder the differentiation and maturation of BMDCs and BMDMs derived from BM cells in vitro. (**A**) Schematic of the overall design of induction of BMDCs and BMDMs from si*CD40*/NP-, si*NC*/NP-, blank NP-, or PBS-treated BM cells. BM cells isolated from C57BL/6 mice were cocultured with si*CD40*/NPs, si*NC*/NPs, blank NPs, or PBS control during BMDCs and BMDMs induction. The siRNA concentration was 50 nM. After culture for 7 days, BMDCs and BMDMs were stimulated with LPS for 24 hours and analyzed by flow cytometry. (**B** to **D**) Frequencies of DCs (B), matured DCs (C), and *CD40*⁺ DCs (D) in BMDCs ($n = 6$ for PBS and blank NPs groups, $n = 4$ for si*NC*/NPs group, and $n = 7$ for si*CD40*/NPs group). (**E** to **G**) Frequencies of macrophages (E), matured macrophages (F), and *CD40*⁺ macrophages (G) in BMDMs ($n = 6$ per group). Data are presented as the means ± SEM. *$P < 0.05$, ****$P < 0.0001$.

DC and macrophage differentiation by affecting their progenitor cells and HSCs. Thus, si*CD40*/NPs may provide a previously unreported avenue for inducing immune tolerance to allograft transplantation. Unlike commonly used immunosuppressive drugs that directly inhibit T cell activation, *CD40*-*CD40*L blockade is more effective in inhibiting APC activation and, hence, T cell priming, favoring tolerance induction (*36*, *37*).

The amount and function of mature APCs, especially DCs, in recipients following transplantation play critical roles in priming alloreactive T cells (*38*). The peripheral DCs and macrophages generally have a short life span; thus, inhibiting the differentiation of HSCs and/or myeloid progenitors toward DCs and macrophages should be more effective in reducing alloreactive T cell activation than targeting mature DCs and macrophages. Because HSCs/progenitor cells reside in their BM niches, HSC- and/or progenitor cell–targeted drug delivery in vivo remains a big challenge (*39*). Although several nanoformulations have been developed for delivering their payloads into HSCs in BM, the drug delivery efficiencies are still unsatisfactory (*40*, *41*). Given that the positive surface charge may enhance the extravasation and penetration abilities

and cellular uptake efficiency of PEGylated nanomedicines in vivo (*42*), cationic NPs were used for RNA delivery in our studies. We found that cationic si*CD40*/NPs exhibited an outstanding drug delivery ability toward both HSCs and myeloid progenitor cells in BM after systemic administration, with an efficiency of approximately 30% in LSK, 29% in CMP, and 60% in GMP, respectively, at 24 hours after a single intravenous injection of the NPs. Thus, siRNA/NPs used in our study offer an effective nanoformulation for regulating gene expression in HSCs and/or myeloid progenitors in vivo.

It is well known that ligation of *CD40* on DCs and macrophages by *CD40*L enhances their antigen-presentation capacity, promotes their maturation, and prolongs their survival (*43*–*45*). A previous in vitro study showed that *CD40* ligation on human *CD34*⁺ cells induced their proliferation and differentiation into functional DCs (*46*). However, because of the low expression levels of *CD40* on HSCs and myeloid progenitors (*47*, *48*), these cells are likely minimally affected by treatment with anti-*CD40* antibodies in vivo. In our study, we successfully delivered *CD40* siRNA into both HSCs and myeloid progenitors in BM by si*CD40*/NPs,

Fig. 7. Lenti-sh*CD40* hinders the differentiation and maturation of DCs and macrophages. (**A**) Schematic of the overall design of the BM cells treated with Lenti-sh*CD40* or Lenti-sh*NC*. BM cells of C57BL/6 mice were cocultured with Lenti-sh*CD40* or Lenti-sh*NC* for 24 hours and cultured for another 7 days. The BMDCs and BMDMs were stimulated with LPS for 24 hours and analyzed by flow cytometry. (**B**) Representative flow cytometry plots demonstrating BMDCs derived from BM cells after culture with Lenti-sh*CD40* or Lenti-sh*NC*. (**C**) Frequencies of *CD40*⁺ DCs derived from BM cells' transfection with Lenti-sh*CD40* or Lenti-sh*NC*. (**D**) MFI of *CD40* of BMDCs. (**E** and **F**) Frequencies of DCs (E) and matured DCs (F) derived from BM cells cultured with Lenti-sh*CD40* or Lenti-sh*NC* after being stimulated with LPS. (**G**) MFI of *CD11c* of BMDCs. [*n* = 5 per group for (C) and (D); *n* = 4 or 6 per group for (E) to (G)]. (**H**) Representative flow cytometry plots demonstrating BMDMs derived from BM cells after culture with Lenti-sh*CD40* or Lenti-sh*NC*. (**I**) Frequencies of CD40⁺ macrophages derived from BM cells' transfection with Lenti-sh*CD40* or Lenti-sh*NC*. (**J**) MFI of *CD40* of BMDMs. (**K** and **L**) Frequencies of macrophages (K) and matured macrophages (L) derived from BM cells cultured with Lenti-sh*CD40* or Lenti-sh*NC* and after being stimulated with LPS. (**M**) MFI of F4/80 of BMDMs [*n* = 3 per group for (I) to (M)]. Data are presented as the means ± SEM. *P < 0.05, **P < 0.01, ***P < 0.001.
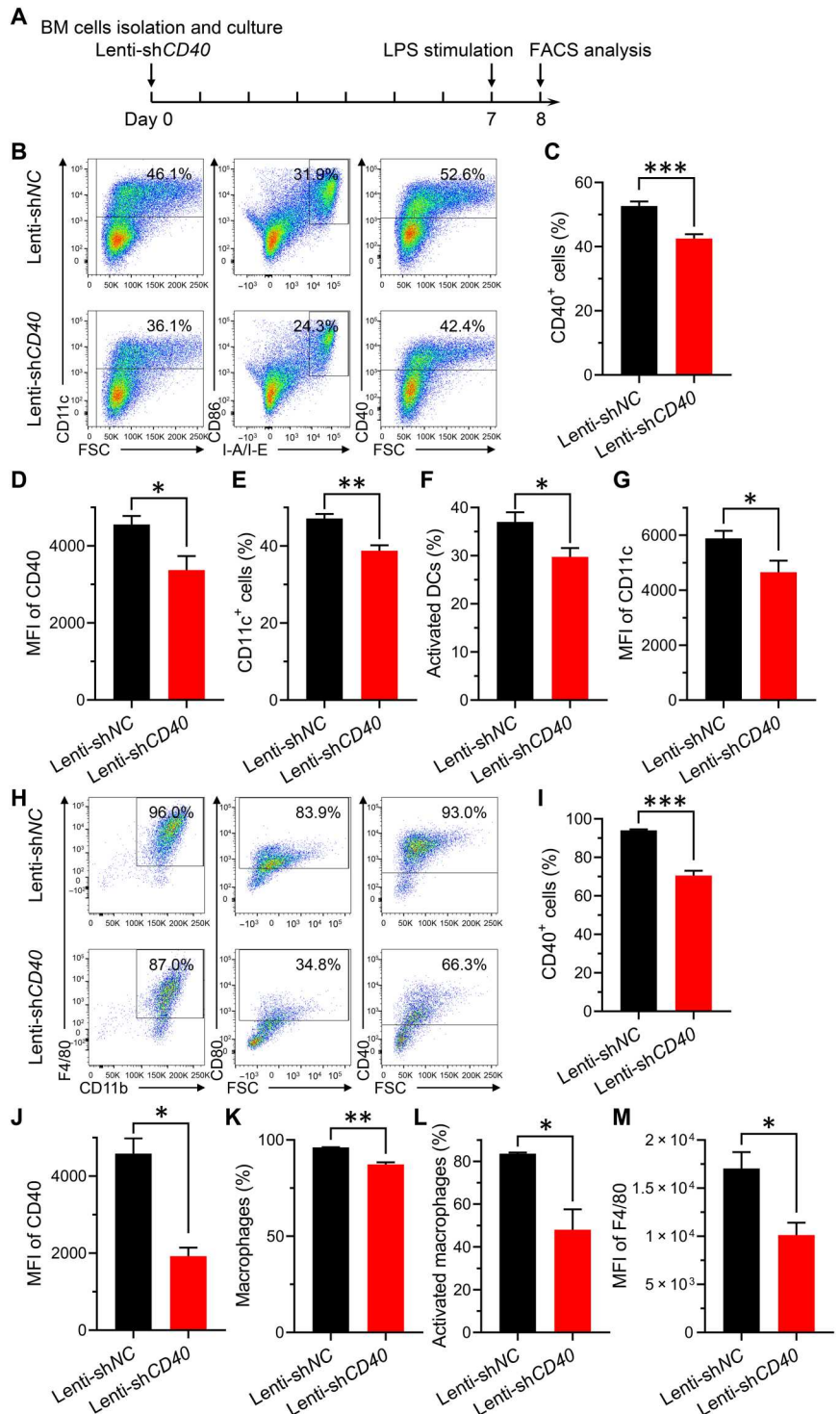
resulting in significant reduction in DCs and macrophages in mice. si*CD40*/NPs treatment notably inhibited the generation of *CD11c*ʰⁱ DCs and F4/80⁺ macrophages, which are highly effective in presenting antigens and activating T cells. DCs and macrophages derived from BM cells of si*CD40*/NP–treated mice displayed a reduced activation against LPS stimulation. The inhibitory effect of *CD40* down-regulation on differentiation of functional DCs and

macrophages was further confirmed by transduction of BM cells with lentivirus-encoding *CD40* shRNA. These results uncovered a previously unappreciated role of the *CD40* signaling pathway in regulating the differentiation of HSCs and myeloid progenitors toward functional DCs and macrophages.

In summary, we have established a promising siRNA delivery system that can efficiently deliver si*CD40* into not only peripheral
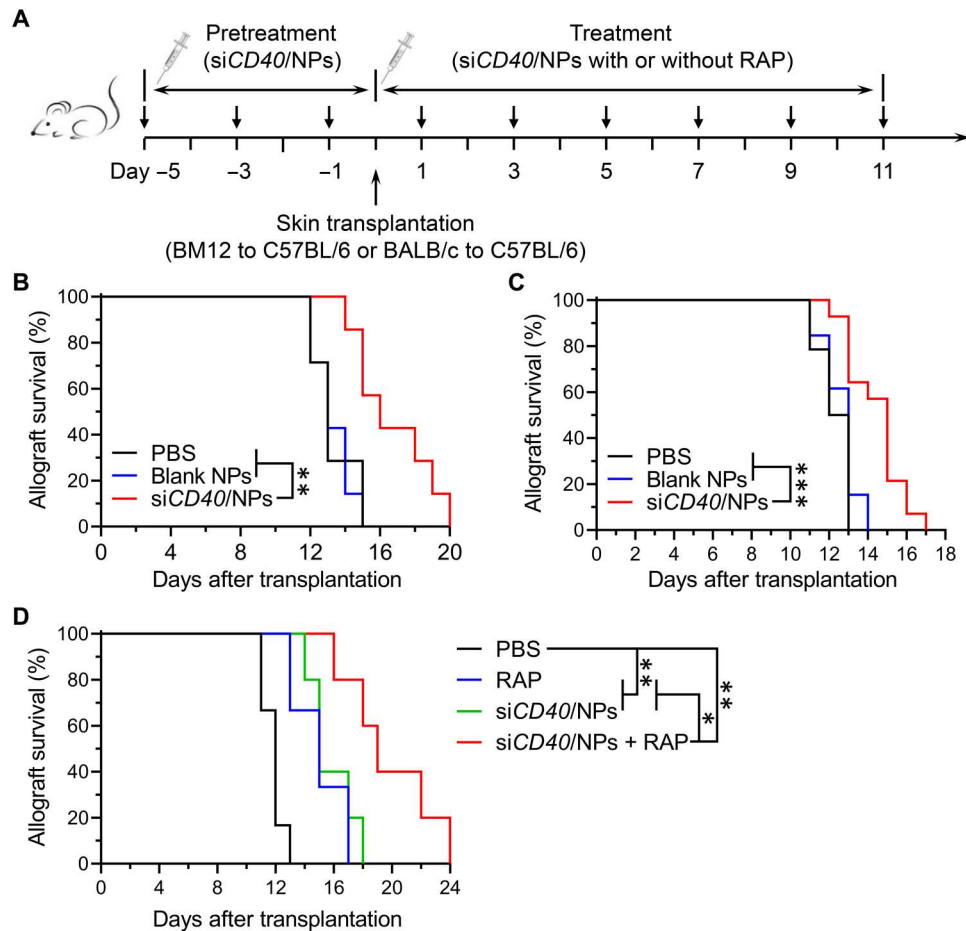
Fig. 8. Significant prolongation of skin allograft survival by si*CD40*/NPs. (**A**) The schematic design of the experiments of mouse allogeneic skin transplantation. C57BL/6 recipient mice were administered nine times with si*CD40*/NPs, blank NPs, or PBS control by intravenous injection every other day. Rapamycin (RAP) was administered (intraperitoneally) six times every other day, starting from 24 hours after skin transplantation. The doses of si*CD40* and rapamycin were 2.5 and 3.0 mg/kg body weight per injection, respectively. The skin grafts from BM12 mice (B) or BALB/c mice (C and D) were transplanted into C57BL/6 mice at 24 hours after the third injection of si*CD40*/NPs, blank NPs, or PBS control. (**B**) Survival curves of MHC class II–mismatched skin allografts ($n = 7$ per group). (**C**) Survival curves of fully MHC plus minor antigen–mismatched skin allografts on C57BL/6 mice ($n = 14$ for PBS and si*CD40*/NPs groups and $n = 13$ for blank NPs group). (**D**) Survival curves of fully MHC plus minor antigen–mismatched skin allografts on C57BL/6 mice ($n = 6$ for PBS and RAP groups and $n = 5$ for si*CD40*/NPs and si*CD40*/NPs + RAP groups). *$P < 0.05$, **$P < 0.01$, ***$P < 0.001$.

DCs and macrophages but also their precursor cells in BM after systemic administration. Using this system, we demonstrate that blockade *CD40* signal pathway in HSCs and myeloid progenitors can significantly inhibit their differentiation toward DCs and macrophages in vivo. Our results highlight the great potential of si*CD40*/NPs in simultaneously significantly reducing the amounts of peripheral DCs and macrophages and their abilities to activate alloreactive T cells, resulting in the suppression of alloimmune responses and prolongation of skin allograft survival in mice.

MATERIALS AND METHODS
Materials
The diblock copolymer of mPEG with PLGA (mPEG$_{5K}$-PLGA$_{10K}$) was provided by J. Wang (South China University of Technology, Guangzhou, China). DOTAP was purchased from Corden Pharma (Liestal, Switzerland). RPMI 1640, L-glutamine, penicillin-streptomycin, fetal bovine serum (FBS), trypan blue, and Lipofectamine 2000 were purchased from Thermo Fisher Scientific

(Waltham, MA, USA). mGM-CSF and mM-CSF were purchased from R&D Systems (Minneapolis, MN, USA). Mouse IL-4 was purchased from PeproTech (Rocky Hill, NJ, USA). siRNA targeting mouse *CD40* mRNA (si*CD40*, antisense strand, 5′-UUCUCAGCC-CAGUGGAACAdTdT-3′), negative control siRNA with a scrambled sequence (si*NC*, antisense strand, 5′-ACGUGACACGUUCGGAGAAdTdT-3′), and fluorescently labeled siRNA (FAM-siRNA and Cy5-siRNA) were synthesized by Suzhou Ribo Life Science Co. (Kunshan, China). Rapamycin was purchased from MCE (Shanghai, China).

Animals
Female C57BL/6 and BALB/c mice (7 to 8 weeks of age) were obtained from Charles River Laboratories (Beijing, China). B6.H-2^{bm12} (BM12) mice (7 to 8 weeks of age) were obtained from the Jackson Laboratory (Bar Harbor, ME, USA). All mice were raised in a specific pathogen–free environment with free access to food and water. All animal protocols were reviewed and approved by the Institutional Animal Care and Use Committee of the First

Hospital of Jilin University, and all experiments were performed in accordance with the protocols.

Preparation of siRNA-encapsulated NPs

NPs with siRNA encapsulation were prepared by a double emulsion solvent evaporation method, as described previously (32). Briefly, 25 μl of ribonuclease-free H_2O containing 200 μg of siRNA was emulsified by sonication (80 W, 60 s) on ice using a Vibra-Cell VCX130 (Sonic & Materials Inc., Newtown, USA) in 500 μl of chloroform containing 3 mg of DOTAP and 25 mg of mPEG-PLGA. The primary emulsion was further emulsified by sonication (80 W, 60 s) on ice in 5 ml of double-distilled H_2O to form a water-in-oil-in-water emulsion. Last, chloroform was removed via rotary evaporation at room temperature using a vacuum Rotavapor (R-210, Buchi, Flawil, Switzerland). The NPs were collected by centrifugation. The diameter and ζ potential of PEG-PLGA NPs were determined using a Zetasizer NanoZS90 (Malvern Instruments, Malvern, UK). The morphologies of si*CD40*/NPs were examined using a cryo-TEM at 200 kV (JEOL 2010, JEOL Ltd., Tokyo, Japan).

Cell culture

The mouse macrophage cell line RAW264.7 and the DC line DC1.2 were purchased from the American Type Culture Collection. These cells were maintained in RPMI 1640 medium supplemented with 10% FBS, 4 mM L-glutamine, and 1% penicillin-streptomycin, and incubated at a 37°C incubator with 5% CO_2. BMDCs or BMDMs were generated by flushing BM cells in the tibia and femur of C57BL/6 mice, followed by culture for 7 days in RPMI 1640 medium supplemented with 10% FBS, mouse IL-4 (10 ng/ml), and GM-CSF (49, 50) or M-CSF (51, 52).

Cellular uptake of NPs

DC1.2 or RAW264.7 (5×10^4) cells were seeded into 24-well plates and cultured for 24 hours to reach 50% confluency. Then, the cells were incubated at 37°C for 2 hours with FAM-siRNA/NPs suspended in complete RPMI 1640 medium at a concentration of FAM-siRNA of 250 nM. PBS, blank NPs, and free FAM-siRNA were used as controls. The medium was aspirated, and cells were rinsed twice with cold PBS. The cells were collected and suspended in 0.025% trypan blue solution for 60 s to quench the nonspecific extracellular fluorescence. The cellular uptake of NPs was determined by flow cytometry.

For fluorescence microscopy observation, DC1.2 and RAW264.7 (5×10^4) cells were seeded into 24-well plates containing a coverslip and cultured for 24 hours to reach 50% confluency. Then, the cells were incubated at 37°C for 2 hours with Cy5-siRNA/NPs suspended in complete RPMI 1640 medium at a concentration of Cy5-siRNA of 250 nM. The medium was aspirated, and cells were washed twice with cold PBS, followed by fixation with acetone for 30 min at −20°C. The cells were further stained with phalloidin-fluorescein isothiocyanate (FITC) (Sigma-Aldrich, St. Louis, MO, USA) for cytoskeleton and 4′,6-diamidino-2-phenylindole (DAPI, Invtrogen, Waltham, MA, USA) for cell nuclei according to the standard protocol provided by the suppliers. The cellular uptake of NPs was visualized by a laser scanning confocal microscope (LSM 880, Zeiss, Jena, Germany).

In vitro gene silencing with si*CD40*/NPs

DC1.2 or RAW264.7 cells were seeded into 24-well plates at 5×10^4 cells per well and cultured overnight at 37°C. The cells were cultured with si*CD40*/NPs at a siRNA dose of 50, 100, or 150 nM. PBS and blank NPs were used as negative controls. Lipofectamine 2000–transfected si*CD40* at a siRNA dose of 75 nM was used as positive control. After 24 and 48 hours of incubation, the cells were harvested, and the expression of *CD40* was determined by qPCR, Western blots, and flow cytometry.

Quantitative real-time PCR

Total RNA from cells treated with si*CD40*/NPs and other controls was extracted using TRIzol (Invtrogen, Waltham, MA, USA) according to the standard protocol provided by the suppliers. Total RNA was transcribed reversely into cDNA using the PrimeScript RT reagent kit with genomic DNA Eraser (Takara, Dalian, China). Then, this cDNA was subjected to qPCR analysis targeting *CD40*, *TNF-α*, *IL-1β*, *IL-6*, *IL-12b*, and *β-actin* using SYBR Premix Ex Taq II (Takara, Dalian, China). The qPCR analysis was performed on the Applied Biosystems StepOnePlus real-time PCR system (Waltham, MA, USA). Relative gene expression values were determined by the ΔΔCt method. Data are presented as the fold difference in *CD40* and proinflammatory cytokine expression normalized to the housekeeping gene β-actin. The primers used in the real-time PCR for *CD40*, *TNF-α*, *IL-1β*, *IL-6*, *IL-12b*, and *β-actin* were as follows: *CD40* forward: 5′-AGCGGTCCATCTAGGG-CAGTGTG-3′, *CD40* reverse: 5′-TGGGTGGCATTGGGTCTTCT-CA-3′; *TNF-α* forward: 5′-CAGGCGGTGCCTATGTCTC-3′, *TNF-α* reverse: 5′-CGATCACCCCGAAGTTCAGTAG-3′; *IL-1β* forward: 5′-GAAATGCCACCTTTTGACAGTG-3′, *IL-1β* reverse: 5′-TGGATGCTCTCATCAGGACAG-3′; *IL-6* forward: 5′-CTGCAA-GAGACTTCCATCCAG-3′, *IL-6* reverse: 5′-AGTGGTATAGA-CAGGTCTGTTGG-3′; *IL-12b* forward: 5′-TGGTTTGCCATCGTTTTGCTG-3′, *IL-12b* reverse: 5′-ACAGGT-GAGGTTCACTGTTTCT-3′; and *β-actin* forward: 5′-ATATCGCTGCGCTGGTCGTC-3′, *β-actin* reverse: 5′-AG-GATGGCGTGAGGGAGAGC-3′.

Western blots

Protein extraction from DC1.2 and RAW264.7 cells treated with si*CD40*/NPs and other controls was performed using radioimmunoprecipitation assay lysis buffer (Beyotime, Shanghai, China) following the manufacturer's protocol. The protein concentration of each sample was determined using the bicinchoninic acid protein assay kit (Pierce/Thermo Fisher Scientific). The protein extracts of each group were fractionated by SDS–polyacrylamide gel electrophoresis and transferred onto a polyvinylidene difluoride membrane. Total *CD40* protein was detected by blotting with anti-mouse *CD40* antibody (Abcam, Cambridge, UK) and peroxidase-conjugated goat anti-rabbit secondary antibody and was visualized with enhanced chemiluminescence substrate (Thermo Fisher Scientific).

In vivo biodistribution of si*CD40*/NPs

Briefly, 16 hours after intravenous injection of Cy5-si*CD40*/NPs or other controls, the peripheral blood cells, splenocytes, and BM cells from the C57BL/6 mice were isolated by erythrocyte lysis as instructed by the manufacturer. The immune cells were stained

with flow cytometry antibodies, and the in vivo cellular uptake of Cy5-si*CD40*/NPs was analyzed by flow cytometry.

For fluorescence microscopy observation, the mouse spleens were fixed in 4% paraformaldehyde and immersed using 30% sucrose solution. Optimal Cutting Temperature (O.C.T.) frozen mouse spleen 4-μm sections were stained with Alexa Fluor 488 anti-mouse *CD68* monoclonal antibody (mAb) (Abcam) and Alexa Fluor 594 anti-mouse *CD11*c (BioLegend) and counterstained with DAPI. The cellular uptake of Cy5-si*CD40*/NPs was visualized by a LSM880 (Zeiss).

For IVIS imaging, C57BL/6 mice were intravenously injected with Cy5-si*CD40*/NPs, free Cy5-si*CD40*, or PBS control. Main organs (brains, lungs, hearts, livers, spleens, and kidneys) and BM cells were taken at 16 hours after Cy5-si*CD40*/NPs administration using the IVIS Spectrum system (PerkinElmer, Waltham, MA, USA). Data were analyzed by the Living Image software (PerkinElmer, Waltham, MA, USA).

Maturation and activation of DCs and macrophages in vivo
C57BL/6 mice were given PBS, si*CD40*/NPs (2.5 mg/kg body weight *CD40* siRNA per mouse), or equivalent blank NPs three times by intravenous injection every other day. Twenty-four hours after the last injection, DCs and macrophages in the spleen were isolated and evaluated by flow cytometry. BMDCs and BMDMs were generated using the isolated BM cells, as described above, and were further stimulated using LPS (1 μg/ml) for 24 hours. Then, these cells were harvested, stained with flow cytometry antibodies, and analyzed by flow cytometry.

Internalization of si*CD40*/NPs by HSCs and myeloid progenitors in vitro
BM cells were isolated from C57BL/6 mice and incubated with Cy5-si*CD40*/NPs and PBS control for 3, 6, or 24 hours. Then, the internalization of Cy5-si*CD40*/NPs by LSK, CMPs, GMPs, monocyte progenitors, and DC progenitors was measured by flow cytometry.

Maturation and activation of DCs and macrophages in vitro
BMDCs and BMDMs were generated with the presence of si*CD40*/NPs, si*NC*/NPs, blank NPs, or PBS control. After culture for 7 days, the BMDCs and BMDMs were further stimulated using LPS (1 μg/ml) for another 24 hours. Then, these cells were harvested and analyzed by flow cytometry. The expression of proinflammatory cytokines in these BMDCs and BMDMs was measured by qPCR.

BMDCs and BMDMs lentivirus transduction
Lentivirus-encoding sh*CD40* (5′-UUCUCAGCCCAGUGGAACA-3′), sh*NC* (5′-ACGUGACACGUUCGGAGAA-3′), and polybrene were obtained from GenePharma (Shanghai, China). BM cells from C57BL/6 mice were transduced with lentivirus at a multiplicity of infection of 10 in the presence of polybrene (5 μg/ml). After incubation at 37°C for 24 hours, the BM cells were washed twice with PBS and cultured with IL-4 and GM-CSF or M-CSF for BMDCs or BMDMs induction, respectively. After culture for 7 days, these BMDCs or BMDMs were further stimulated using LPS (1 μg/ml) for another 24 hours. The differentiation and maturation of DCs and macrophages were analyzed by flow cytometry.

Flow cytometric analysis
Flow cytometry was used to determine the cellular uptake of NPs and phenotypes of mouse immune cells using various combinations of the following fluorescence-labeled anti-mouse mAbs: CD3 (17A2), CD4 (GK1.5), CD8 (53-6.7), CD11b (M1/70), CD11c (N418), CD16/32(93), CD19 (6D5), CD25 (PC61), CD34(SA376A4), CD40 (3/23), CD45 (30-F11), CD80 (16-10A1), CD86 (GL-1), CD115(AFS98), CD117 (c-Kit, 2B8), F4/80 (BM8), I-A/I-E (M5/114.15.2), Ly-6C (HK1.4), NK1.1 (PK136), and Sca-1(D7). Biotin anti-mouse lineage panel from BioLegend (San Diego, CA, USA) was used in accordance with the manufacturer's protocol. Single-cell suspensions were stained with flow cytometric antibodies for 30 min at 4°C. All samples were acquired on a BD LSR Fortessa (BD Bioscience, San Jose, CA, USA). The data were analyzed by FlowJo software (TreeStar, San Carlos, CA, USA).

Skin graft transplantation
Female C57BL/6 mice were given PBS, si*CD40*/NPs, or blank NPs nine times every other day. The dose of si*CD40* was 2.5 mg/kg body weight per injection. Rapamycin was administered six times at a dose of 3 mg/kg body weight by intraperitoneal injection every other day starting from 24 hours after skin transplantation. The skin grafts from BM12 mice or BALB/c mice were transplanted into C57BL/6 recipients, as described previously (*53*). Briefly, C57BL/6 mice were placed prone and a 5 × 10-mm piece of skin was removed from the middle dorsal thorax over the costal margin. The 5 × 10-mm pieces of skin from BM12 mice or BALB/c mice were then fashioned and their edges were sutured to the C57BL/6 mice recipient skin with a non-absorbable 5-0 prolene suture (Jinhuan, Shanghai, China). Grafts were fenestrated and covered with a povidone-iodine mesh and pressure dressing and secured with circumferential tape. Bandages were left in place for 7 days and then removed under general anesthetic. Skin grafts were monitored every day until less than 10% of the graft remained viable, which was defined as complete loss.

MLR assay
The responder leukocytes (4×10^5 per well) obtained from the spleens and lymph nodes of C57BL/6 recipient mice on the 7th day after skin graft transplantation were cocultured with irradiated (30 gray) stimulator spleen cells (4×10^5 per well) in flat-bottomed 96-well plates for 3 days. BrdU (5-bromo-2′-deoxyuridine) labeling solution was added to culture medium. These cells were incubated for a further 18 hours and harvested on day 4. Cell proliferation was measured using a colorimetric BrdU cell proliferation kit (Roche, Basel, Switzerland) according to the manufacturer's instructions. Results were expressed as stimulation index (SI). The SI was calculated as follows: SI = absorbance value of allogeneic MLR/absorbance value of syngeneic MLR.

Histopathology
The skin allografts were collected from C57BL/6 recipient mice 7 days after skin graft transplantation. The brains, lungs, hearts, livers, spleens, and kidneys were obtained from C57BL/6 recipient mice at the end of the skin graft transplantation experiment. All these tissues were fixed in 4% paraformaldehyde. The paraffin-embedded tissues were sliced into 2.5-μm-thick sections and stained with hematoxylin and eosin and photographed using a microscope.

Statistical analysis

Statistics were performed on GraphPad Prism 8, and Student's *t* tests or one-way analysis of variance was used to compare the paired and unpaired analyses. The statistical evaluation of mouse skin allograft survival was performed using the log-rank test. *P* values < 0.05 were considered statistically significant.

Supplementary Materials

This PDF file includes:
Figs. S1 to S10

View/request a protocol for this paper from *Bio-protocol*.

REFERENCES AND NOTES

1. A. Loupy, C. Lefaucheur, Antibody-mediated rejection of solid-organ allografts. *N. Engl. J. Med.* **379**, 1150–1160 (2018).
2. J. Stolp, M. Zaitsu, K. J. Wood, Immune tolerance and rejection in organ transplantation. *Methods Mol. Biol.* **1899**, 159–180 (2019).
3. J. Ochando, Z. A. Fayad, J. C. Madsen, M. G. Netea, W. J. M. Mulder, Trained immunity in organ transplantation. *Am. J. Transplant.* **20**, 10–18 (2020).
4. D. Bezinover, F. Saner, Organ transplantation in the modern era. *BMC Anesthesiol.* **19**, 32 (2019).
5. S. Cai, A. Chandraker, Cell therapy in solid organ transplantation. *Curr. Gene Ther.* **19**, 71–80 (2019).
6. Q. Zhuang, Q. Liu, S. J. Divito, Q. Zeng, K. M. Yatim, A. D. Hughes, D. M. Rojas-Canales, A. Nakao, W. J. Shufesky, A. L. Williams, R. Humar, R. A. Hoffman, W. D. Shlomchik, M. H. Oberbarnscheidt, F. G. Lakkis, A. E. Morelli, Graft-infiltrating host dendritic cells play a key role in organ transplant rejection. *Nat. Commun.* **7**, 12623 (2016).
7. H. Hasegawa, T. Matsumoto, Mechanisms of tolerance induction by dendritic cells in vivo. *Front. Immunol.* **9**, 350 (2018).
8. A. E. Morelli, A. W. Thomson, Tolerogenic dendritic cells and the quest for transplant tolerance. *Nat. Rev. Immunol.* **7**, 610–621 (2007).
9. J. Banchereau, R. M. Steinman, Dendritic cells and the control of immunity. *Nature* **392**, 245–252 (1998).
10. F. Ordikhani, V. Pothula, R. Sanchez-Tarjuelo, S. Jordan, J. Ochando, Macrophages in organ transplantation. *Front. Immunol.* **11**, 582939 (2020).
11. T. P. van den Bosch, N. M. Kannegieter, D. A. Hesselink, C. C. Baan, A. T. Rowshani, Targeting the monocyte-macrophage lineage in solid organ transplantation. *Front. Immunol.* **8**, 153 (2017).
12. L. Chen, D. B. Flies, Molecular mechanisms of T cell co-stimulation and co-inhibition. *Nat. Rev. Immunol.* **13**, 227–242 (2013).
13. A. G. Baxter, P. D. Hodgkin, Activation rules: The two-signal theories of immune activation. *Nat. Rev. Immunol.* **2**, 439–446 (2002).
14. D. F. Pinelli, M. L. Ford, Novel insights into anti-CD40/CD154 immunotherapy in transplant tolerance. *Immunotherapy* **7**, 399–410 (2015).
15. P. Malvezzi, T. Jouve, L. Rostaing, Costimulation blockade in kidney transplantation: An update. *Transplantation* **100**, 2315–2323 (2016).
16. C. P. Larsen, E. T. Elwood, D. Z. Alexander, S. C. Ritchie, R. Hendrix, C. Tucker-Burden, H. R. Cho, A. Aruffo, D. Hollenbaugh, P. S. Linsley, K. J. Winn, T. C. Pearson, Long-term acceptance of skin and cardiac allografts after blocking CD40 and CD28 pathways. *Nature* **381**, 434–438 (1996).
17. A. D. Kirk, L. C. Burkly, D. S. Batty, R. E. Baumgartner, J. D. Berning, K. Buchanan, J. H. Fechner Jr., R. L. Germond, R. L. Kampen, N. B. Patterson, S. J. Swanson, D. K. Tadaki, C. N. TenHoor, L. White, S. J. Knechtle, D. M. Harlan, Treatment with humanized monoclonal antibody against CD154 prevents acute renal allograft rejection in nonhuman primates. *Nat. Med.* **5**, 686–693 (1999).
18. S. C. Kim, W. Wakwe, L. B. Higginbotham, D. V. Mathews, C. P. Breeden, A. C. Stephenson, J. Jenkins, E. Strobert, K. Price, L. Price, R. Kuhn, H. Wang, A. Yamniuk, S. Suchard, A. B. Farris III, T. C. Pearson, C. P. Larsen, M. L. Ford, A. Suri, S. Nadler, A. B. Adams, Fc-silent anti-CD154 domain antibody effectively prevents nonhuman primate renal allograft rejection. *Am. J. Transplant.* **17**, 1182–1192 (2017).
19. T. Kawai, D. Andrews, R. B. Colvin, D. H. Sachs, A. B. Cosimi, Thromboembolic complications after treatment with monoclonal antibody against CD40 ligand. *Nat. Med.* **6**, 114 (2000).
20. F. Cordoba, G. Wieczorek, M. Audet, L. Roth, M. A. Schneider, A. Kunkler, N. Stuber, M. Erard, M. Ceci, R. Baumgartner, R. Apolloni, A. Cattini, G. Robert, D. Ristig, J. Munz, L. Haeberli,

R. Grau, D. Sickert, C. Heusser, P. Espie, C. Bruns, D. Patel, J. S. Rush, A novel, blocking, Fc-silent anti-CD40 monoclonal antibody prolongs nonhuman primate renal allograft survival in the absence of B cell depletion. *Am. J. Transplant.* **15**, 2825–2836 (2015).
21. I. R. Badell, P. W. Thompson, A. P. Turner, M. C. Russell, J. G. Avila, J. A. Cano, J. M. Robertson, F. V. Leopardi, E. A. Strobert, N. N. Iwakoshi, K. A. Reimann, M. L. Ford, A. D. Kirk, C. P. Larsen, Nondepleting anti-CD40-based therapy prolongs allograft survival in nonhuman primates. *Am. J. Transplant.* **12**, 126–135 (2012).
22. C. van Kooten, J. Banchereau, CD40-CD40 ligand. *J. Leukoc. Biol.* **67**, 2–17 (2000).
23. J. Suttles, R. D. Stout, Macrophage CD40 signaling: A pivotal regulator of disease protection and pathogenesis. *Semin. Immunol.* **21**, 257–264 (2009).
24. T. R. Brummelkamp, R. Bernards, R. Agami, A system for stable expression of short interfering RNAs in mammalian cells. *Science* **296**, 550–553 (2002).
25. N. S. Lee, T. Dohjima, G. Bauer, H. Li, M. J. Li, A. Ehsani, P. Salvaterra, J. Rossi, Expression of small interfering RNAs targeted against HIV-1 rev transcripts in human cells. *Nat. Biotechnol.* **20**, 500–505 (2002).
26. Y. Dong, D. J. Siegwart, D. G. Anderson, Strategies, design, and chemistry in siRNA delivery systems. *Adv. Drug Deliv. Rev.* **144**, 133–147 (2019).
27. S. Yonezawa, H. Koide, T. Asai, Recent advances in siRNA delivery mediated by lipid-based nanoparticles. *Adv. Drug Deliv. Rev.* **154-155**, 64–78 (2020).
28. B. Kim, J. H. Park, M. J. Sailor, Rekindling RNAi therapy: Materials design requirements for in vivo siRNA delivery. *Adv. Mater.* **31**, e1903637 (2019).
29. R. Kanasty, J. R. Dorkin, A. Vegas, D. Anderson, Delivery materials for siRNA therapeutics. *Nat. Mater.* **12**, 967–977 (2013).
30. A. Jorge, A. Pais, C. Vitorino, Targeted siRNA delivery using lipid nanoparticles. *Methods Mol. Biol.* **2059**, 259–283 (2020).
31. J. Majumder, O. Taratula, T. Minko, Nanocarrier-based systems for targeted and site specific therapeutic delivery. *Adv. Drug Deliv. Rev.* **144**, 57–77 (2019).
32. X. Z. Yang, S. Dou, T. M. Sun, C. Q. Mao, H. X. Wang, J. Wang, Systemic delivery of siRNA with cationic lipid assisted PEG-PLA nanoparticles for cancer therapy. *J. Control. Release* **156**, 203–211 (2011).
33. S. M. Hartig, R. R. Greene, G. Carlesso, J. N. Higginbotham, W. N. Khan, A. Prokop, J. M. Davidson, Kinetic analysis of nanoparticulate polyelectrolyte complex interactions with endothelial cells. *Biomaterials* **28**, 3843–3855 (2007).
34. I. R. Ferrer, M. E. Wagener, M. Song, A. D. Kirk, C. P. Larsen, M. L. Ford, Antigen-specific induced Foxp3⁺ regulatory T cells are generated following CD40/CD154 blockade. *Proc. Natl. Acad. Sci. U.S.A.* **108**, 20701–20706 (2011).
35. D. Liu, I. R. Ferrer, M. Konomos, M. L. Ford, Inhibition of CD8+ T cell-derived CD40 signals is necessary but not sufficient for Foxp3+ induced regulatory T cell generation in vivo. *J. Immunol.* **191**, 1957–1964 (2013).
36. C. Guillot, C. Guillonneau, P. Mathieu, C. A. Gerdes, S. Ménoret, C. Braudeau, L. Tesson, K. Renaudin, M. G. Castro, P. R. Löwenstein, I. Anegon, Prolonged blockade of CD40-CD40 ligand interactions by gene transfer of CD40Ig results in long-term heart allograft survival and donor-specific hyporesponsiveness, but does not prevent chronic rejection. *J. Immunol.* **168**, 1600–1609 (2002).
37. P. F. Halloran, Immunosuppressive drugs for kidney transplantation. *N. Engl. J. Med.* **351**, 2715–2729 (2004).
38. R. Lechler, W. F. Ng, R. M. Steinman, Dendritic cells in transplantation—Friend or foe? *Immunity* **14**, 357–368 (2001).
39. C. F. Mu, J. Shen, J. Liang, H. S. Zheng, Y. Xiong, Y. H. Wei, F. Li, Targeted drug delivery for tumor therapy inside the bone marrow. *Biomaterials* **155**, 191–202 (2018).
40. R. Bahal, N. Ali McNeer, E. Quijano, Y. Liu, P. Sulkowski, A. Turchick, Y. C. Lu, D. C. Bhunia, A. Manna, D. L. Greiner, M. A. Brehm, C. J. Cheng, F. López-Giráldez, A. Ricciardi, J. Beloor, D. S. Krause, P. Kumar, P. G. Gallagher, D. T. Braddock, W. Mark Saltzman, D. H. Ly, P. M. Glazer, In vivo correction of anaemia in β-thalassemic mice by γPNA-mediated gene editing with nanoparticle delivery. *Nat. Commun.* **7**, 13304 (2016).
41. H. K. Mandl, E. Quijano, H. W. Suh, E. Sparago, S. Oeck, M. Grun, P. M. Glazer, W. M. Saltzman, Optimizing biodegradable nanoparticle size for tissue-specific delivery. *J. Control. Release* **314**, 92–101 (2019).
42. H.-X. Wang, Z.-Q. Zuo, J.-Z. Du, Y.-C. Wang, R. Sun, Z.-T. Cao, X.-D. Ye, J.-L. Wang, K. W. Leong, J. Wang, Surface charge critically affects tumor penetration and therapeutic efficacy of cancer nanomedicines. *Nano Today* **11**, 133–144 (2016).
43. S. P. Schoenberger, R. E. Toes, E. I. van der Voort, R. Offringa, C. J. Melief, T-cell help for cytotoxic T lymphocytes is mediated by CD40–CD40L interactions. *Nature* **393**, 480–483 (1998).
44. I. S. Grewal, R. A. Flavell, CD40 and CD154 in cell-mediated immunity. *Annu. Rev. Immunol.* **16**, 111–135 (1998).
45. R. Elgueta, M. J. Benson, V. C. de Vries, A. Wasiuk, Y. Guo, R. J. Noelle, Molecular mechanism and function of CD40/CD40L engagement in the immune system. *Immunol. Rev.* **229**, 152–172 (2009).

46. L. Flores-Romo, P. Björck, V. Duvert, C. van Kooten, S. Saeland, J. Banchereau, CD40 ligation on human cord blood CD34^{+} hematopoietic progenitors induces their proliferation and differentiation into functional dendritic cells. *J. Exp. Med.* **185**, 341–349 (1997).

47. D. Rondelli, R. M. Lemoli, M. Ratta, M. Fogli, F. Re, A. Curti, M. Arpinati, S. Tura, Rapid induction of CD40 on a subset of granulocyte colony-stimulating factor–mobilized CD34^{+} blood cells identifies myeloid committed progenitors and permits selection of nonimmunogenic CD40^{–} progenitor cells. *Blood* **94**, 2293–2300 (1999).

48. I. Mavroudi, V. Papadaki, K. Pyrovolaki, P. Katonis, A. G. Eliopoulos, H. A. Papadaki, The CD40/CD40 ligand interactions exert pleiotropic effects on bone marrow granulopoiesis. *J. Leukoc. Biol.* **89**, 771–783 (2011).

49. J. I. Mayordomo, T. Zorina, W. J. Storkus, L. Zitvogel, C. Celluzzi, L. D. Falo, C. J. Melief, S. T. Ildstad, W. M. Kast, A. B. Deleo, M. T. Lotze, Bone marrow-derived dendritic cells pulsed with synthetic tumour peptides elicit protective and therapeutic antitumour immunity. *Nat. Med.* **1**, 1297–1302 (1995).

50. Y. I. Son, S. Egawa, T. Tatsumi, R. E. Redlinger Jr., P. Kalinski, T. Kanto, A novel bulk-culture method for generating mature dendritic cells from mouse bone marrow cells. *J. Immunol. Methods* **262**, 145–157 (2002).

51. W. Ying, P. S. Cheruku, F. W. Bazer, S. H. Safe, B. Zhou, Investigation of macrophage polarization using bone marrow derived macrophages. *J. Vis. Exp.* , e50323 (2013).

52. G. Zhuang, C. Meng, X. Guo, P. S. Cheruku, L. Shi, H. Xu, H. Li, G. Wang, A. R. Evans, S. Safe, C. Wu, B. Zhou, A novel regulator of macrophage activation: miR-223 in obesity-associated adipose tissue inflammation. *Circulation* **125**, 2892–2903 (2012).

53. F. Issa, J. Hester, R. Goto, S. N. Nadig, T. E. Goodacre, K. Wood, Ex vivo-expanded human regulatory T cells prevent the rejection of skin allografts in a humanized mouse model. *Transplantation* **90**, 1321–1327 (2010).